

Braiding of Majorana corner states in electric circuits and its non-Hermitian generalization

Motohiko Ezawa

Department of Applied Physics, University of Tokyo, Hongo 7-3-1, 113-8656, Japan

We propose to realize Majorana edge and corner states in electric circuits. First, we simulate the Kitaev model by an LC electric circuit and the $p_x + ip_y$ model by an LC circuit together with operational amplifiers. Zero-energy edge states emerge in the topological phase, which are detectable by measuring impedance. Next, we simulate the Bernevig-Hughes-Zhang model by including an effective magnetic field without breaking the particle-hole symmetry, where zero-energy corner states emerge in the topological phase. It is demonstrated that they are Ising anyons subject to the braiding. Namely we derive $\sigma^2 = -1$ for them, where σ denotes the single-exchange operation. They may well be called Majorana states. We also study non-Hermitian generalizations of these models by requiring the particle-hole symmetry. It is shown that the braiding holds in certain reciprocal non-Hermitian generalizations.

Introduction: A Majorana state will be a key for future topological quantum computations¹ owing to the braiding. Majorana states are realized in topological superconductors^{2,3} and Kitaev spin liquids^{4,5}. In these systems, the particle-hole symmetry (PHS) plays an essential role since the zero-energy states becomes Majorana states⁶⁻⁸. Recently, Majorana corner states are proposed in various systems⁹⁻¹⁵, where the braiding has been shown for some of them^{14,15}. Furthermore, Majorana states in non-Hermitian systems are studied in various contexts¹⁶⁻²⁵. It is an interesting problem to seek other systems realizing Majorana states. Especially, it is fascinating if Majorana states are simulated by electric circuits.

Various topological phases are realized in electric circuits, such as the SSH model²⁶, graphene^{26,27}, Weyl semimetal^{26,28}, nodal-line semimetal^{29,30}, higher-order topological phases³¹⁻³³, Chern insulators³⁴ and non-Hermitian topological phases^{35,36}. A topological phase transition is induced by tuning variable capacitors and inductors. The impedance signals the edge and corner states^{26,27,31-36}.

In this paper, we propose to realize Majorana edge states and corner states in electric circuits. The essence is that parameters are tunable to make the system respect the PHS. First, we simulate the Kitaev model either by a pure LC circuit or by an LC circuit together with operational amplifiers. The $p_x + ip_y$ model is also constructed by aligning these two circuits along the orthogonal directions. Zero-energy edge states corresponding to Majorana states are well observed by measuring the impedance. Next, we simulate the Bernevig-Hughes-Zhang (BHZ) model together with an effective Zeeman field by an electric circuit. The model corresponds to a second-order topological superconductor with the emergence of a pair of Majorana corner states. We demonstrate explicitly that the braiding holds between a pair of corner states by calculating the Berry phase in an electric circuit.

The introduction of resistance makes the electric circuit non-Hermitian due to the Joule loss³⁵. There are two types of non-Hermitian models, i.e., reciprocal models and nonreciprocal models, where nonreciprocity indicates that the forward and backward hopping amplitudes are different between two nodes. As far as the PHS is respected, it is shown that the braiding holds for the two corner states in a reciprocal non-Hermitian extension of the BHZ model. However, the braiding becomes meaningless in the nonreciprocal extension.

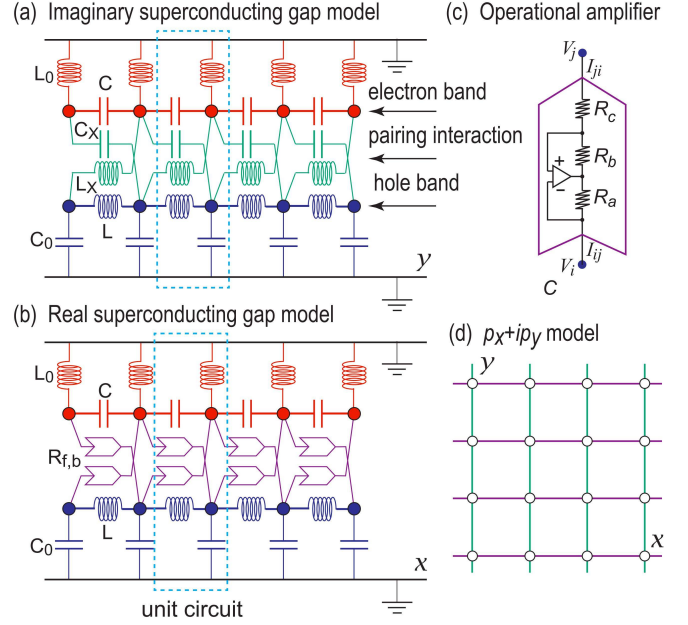


FIG. 1: Minimal electronic circuits realizing the Kitaev model. Each circuit consists of two main wires colored in red and blue, simulating electron and hole bands, respectively. The unit cell is shown by a dotted cyan box, and contains two nodes colored in red and blue. (a) Imaginary superconducting gap model is realized by a pure LC circuit. (b) Real superconducting gap model is realized by an additional use of operational amplifiers. (c) Structure of an operational amplifier. (d) The $p_x + ip_y$ model is constructed so that the 1D circuits (a) and (b) are aligned in the x and y directions, respectively. Green and purple links represent pairing interactions of the types (a) and (b), respectively.

Electric-circuit realization of the Kitaev model: The Kitaev p -wave topological superconductor model is the fundamental model hosting Majorana zero-energy edge states in one dimensional (1D) space. The model is represented in the two forms, i.e., by the Hamiltonian H^y with the imaginary superconducting pairing, and H^x with the real superconducting pairing. It consists of the hopping term H_t and the superconducting interaction term H_{SC}^i , where

$$H^i = H_t \sigma_z + H_{SC}^i, \quad (1)$$

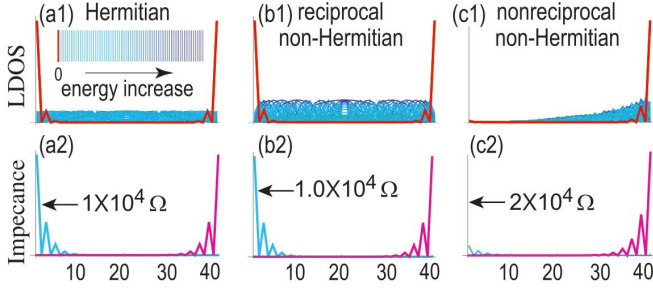


FIG. 2: (a1)–(c1) LDOS of a finite chain of the Hermitian and non-Hermitian Kitaev models with length $N = 40$ in the topological phase, where the red peaks at the edges represent zero-energy edge states. Skin states are observed in the nonreciprocal system (c1). The energy of the state is represented by a color subject to the color palette in the inset of (a1). (a2)–(c2) Two-point impedance of the corresponding LC circuit with operational amplifiers, where the peaks at the edges are due to zero-energy edge states. The horizontal axis is the site index. Magenta (cyan) curves indicate the impedance when one node is fixed at the left (right) edge. The parameters are as follows: $t = 1$, $\Delta = 0.5$ and $\mu = 0$ for the Kitaev model (a); $t = 1 + 0.2i$, $\Delta = 0.5$ and $\mu = 0$ for the reciprocal non-Hermitian Kitaev model (b); $t = 1$, $\Delta^f = 0.5$, $\Delta^b = 0.3$ and $\mu = 0$ for the nonreciprocal non-Hermitian Kitaev model (c).

with

$$H_t = -t \cos k - \mu, \quad (2)$$

$$H_{SC}^y = \Delta_y \sigma_y \sin k, \quad H_{SC}^x = \Delta_x \sigma_x \sin k. \quad (3)$$

Here, t , μ and Δ_i represent the hopping amplitude, the chemical potential and the superconducting gap parameter. It is a two-band model, and the Hamiltonian is a 2×2 matrix. It is well known that the system is topological for $|\mu| < |2t|$ and trivial for $|\mu| > |2t|$ irrespective of Δ_i provided $\Delta_i \neq 0$.

We simulate the Kitaev model by electric circuits. There are two types of circuits corresponding to the two Hamiltonians H^y and H^x , as illustrated in Fig.1(a) and (b).

Let us explain how to construct them. We use two main wires to represent a two-band model: One wire consists of capacitors C in series, implementing the electron band, while the other wire consists of inductors L in series, implementing the hole band. The hopping parameters are opposite between the electron and hole bands, which are represented by capacitors and inductors. Indeed, they contribute the terms proportional to $i\omega C$ and $1/(i\omega L)$ to the circuit Laplacian $J_{ab}(\omega)$ in (4), respectively, where ω is the frequency of the AC current.

In the wire with capacitors (inductors), each node a is connected to the ground via an inductor L_0 (C_0), as in Fig.1(a)–(b). This setting is made to make the system topological.

We then introduce pairing interactions between them. In order to construct the model H^y , we cross bridge two wires by capacitors C_X and inductors L_X as shown in Fig.1(a). On the other hand, in order to construct the model H^x , we cross bridge two wires by operational amplifiers, which act as negative impedance converters with current inversion³⁴. In the operational amplifier, the resistance depends on the current flowing direction; R_f for the forward flow and $-R_b$ for

the backward flow with the convention that $R_b > 0$. We set $R_X = R_f = R_b$ to make the system reciprocal. A generalization to the nonreciprocal theory with $R_f \neq R_b$ is straightforward.

The unit cell indicated by a dotted cyan box contains two sites in Fig.1. Accordingly, we set $I_a = (I_a^L, I_a^C)$ and $V_a = (V_a^L, V_a^C)$, where $I_a^{L(C)}$ is the current between node $a^{L(C)}$ and the ground via the inductance L (conductance C), and $V_a^{L(C)}$ is the voltage at node $a^{L(C)}$.

When we apply an AC voltage $V(t) = V(0)e^{i\omega t}$, the Kirchhoff current law leads to the following formula^{26,31},

$$I_a(\omega) = \sum_b J_{ab}(\omega) V_b(\omega), \quad (4)$$

where the sum is taken over all adjacent nodes b , and $J_{ab}(\omega)$ is called the circuit Laplacian.

(i) In the case of the circuit in Fig.1(a) we explicitly obtain

$$J = \begin{pmatrix} f_1 & g_1 \\ g_2 & f_2 \end{pmatrix}, \quad (5)$$

with

$$\begin{aligned} f_1 &= -2C \cos k + 2C - (\omega^2 L_0)^{-1}, \\ f_2 &= 2(\omega^2 L)^{-1} \cos k - 2(\omega^2 L)^{-1} + C_0, \\ g_1 &= -C_X e^{ik} + (\omega^2 L_X)^{-1} e^{-ik}, \\ g_2 &= (\omega^2 L_X)^{-1} e^{ik} - C_X e^{-ik}, \end{aligned} \quad (6)$$

describing the imaginary superconducting pairing model H^y .

(ii) In the case of the circuit in Fig.1(b) we explicitly obtain (5), where f_1 and f_2 are given by (6) and

$$g_1 = g_2 = (i\omega R_b)^{-1} e^{ik} - (i\omega R_f)^{-1} e^{-ik}, \quad (7)$$

describing the real superconducting pairing model H^x .

The key procedure is to equate the circuit Laplacian (5) with the Hamiltonian (1). In so doing, it is necessary to require the PHS for the circuit, which requires us to tune the parameters to satisfy $\omega_0 \equiv 1/\sqrt{LC} = 1/\sqrt{L_0 C_0} = 1/\sqrt{L_X C_X}$, and set the AC frequency as $\omega = \omega_0$. At this frequency, we may set $J_{ab}(\omega) = i\omega H_{ab}^i(\omega)$, which dictates the correspondence between the circuit and the superconductor model as $t = -C$, $\mu = -2C + C_0$, $\Delta_y = C_X$, and $\Delta_x = (\omega_0 R_X)^{-1}$.

The system is precisely at the topological phase-transition point $|\mu| = |2t|$ without the capacitors C_0 and the inductors L_0 , since the condition $\mu = -2t$ is satisfied. It is topological in the presence of C_0 and L_0 . The system turns into a trivial phase when we exchange the capacitors C_0 and inductors L_0 connected to ground.

By calculating the LDOS as in Fig.2(a1), we find the emergence of the zero-energy edge states in the topological phase. They are observable by measuring the impedance between the a and b nodes, which is given by²⁷ $Z_{ab} \equiv V_a/I_b = G_{ab}$, where G is the Green function defined by the inverse of the Laplacian J , $G \equiv J^{-1}$. We show numerical results in Fig.2(a2) for typical values of parameters, where we have set one node at the left or right edge. The behavior of the impedance is very similar to that of the LDOS.

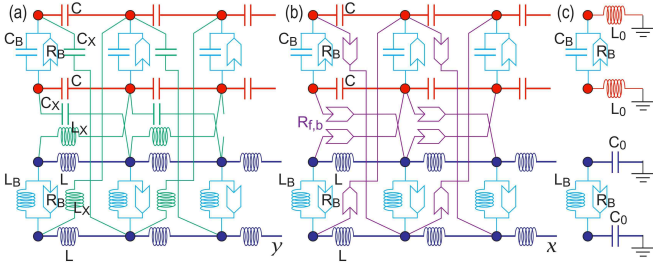


FIG. 3: Electric-circuit realization of the BHZ model together with effective field B . The B field is simulated by parts involving (C_B, R_B) and (L_B, R_B) colored in cyan. (a) 2D view into the x direction. (b) 2D view into the y direction. (c) Each node is connected to the ground by an inductor or a capacitor in (a) and (b). We have set $t = 1, \mu = 1, \Delta = 1$ and $B = 1/2$.

(iii) We next consider the $p_x + ip_y$ model, whose Hamiltonian is given by (1) with

$$H_t = t(\cos k_x + \cos k_y) - \mu, \quad (8)$$

$$H_{SC} = \Delta(\sigma_x \sin k_x + \sigma_y \sin k_y). \quad (9)$$

The model is simulated by layering the circuit for H^y in the x direction and the circuit for H^x in the y direction as shown in Fig.1(d). The relations between the parameters are given by

$$t = -C, \quad \mu = -2C + C_0, \quad \Delta = C_X = (\omega_0 R_X)^{-1}. \quad (10)$$

It is a topological superconductor for $|\mu| < |2t|$, where the zero-energy edge states emerge along all four edges.

Braiding of Majorana corner states: The zero-energy edge states are Majorana states in the Kitaev model, but it is not easy to study the braiding³⁷ in the electric-circuit formalism. The zero-energy edge states in $p_x + ip_y$ model is 2D. We proceed to investigate a 2D model possessing a pair of zero-energy corner states to explore the braiding.

Such a model is given by the Bernevig-Hughes-Zhang Hamiltonian³⁸, $H^{\text{BHZ}} = H_t \tau_z + H_{SO} \tau_x$, where H_t and H_{SO} are given by (8) and (9), respectively. Although it is proposed for a topological insulator, it has the PHS, $\Xi^{-1} H(\mathbf{k}) \Xi = -H(-\mathbf{k})$ with $\Xi = \tau_y \sigma_y K$, where K represents complex conjugation. When the Zeeman term $H_Z = B(\sigma_x \cos \theta + B \sigma_y \sin \theta)$ is applied, it becomes a second-order topological superconductor with the emergence of zero-energy topological corner states^{14,39}. However, it breaks the PHS¹². Here we propose the term $H_{\tau Z} = B \tau_z (\sigma_x \cos \theta + \sigma_y \sin \theta)$, which respects the PHS. Such a term does not exist in condensed matter, but it is allowed in electric circuits: See cyan parts in Fig.3.

We simulate the BHZ model with the B field, $H_{\tau Z}^{\text{BHZ}}(\theta) \equiv H^{\text{BHZ}} + H_{\tau Z}$, by an electric circuit. It is straightforward to generalize the above circuits in Fig.1 to the present one as in Fig.3. Since it is a four-band model, we use four main wires. By analyzing the Kirchhoff current law, we may derive the circuit Laplacian $J_{ab}(\omega)$, which is now a 4×4 matrix. Solving $J_{ab}(\omega) = i\omega H_{\tau Z}^{\text{BHZ}}$, we obtain the correspondence between the system parameters. They are given by (10) supplemented by $B_x = C_B$ or L_B and $B_y = R_B$ for the B field. We show

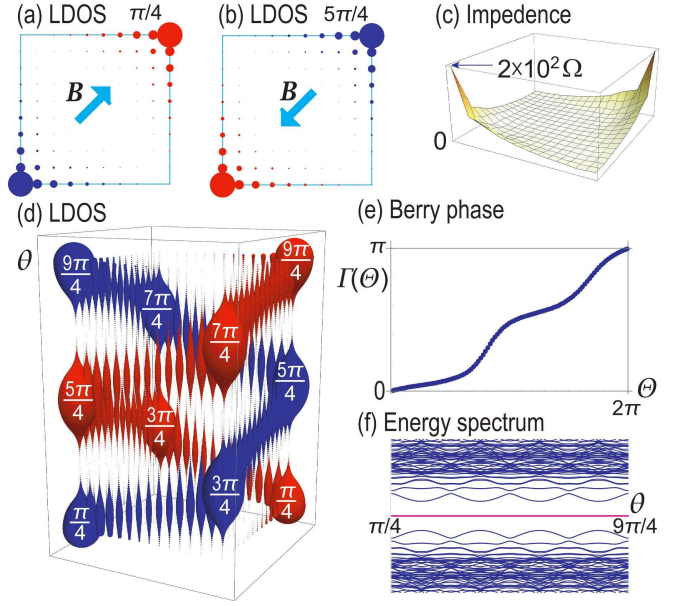


FIG. 4: LDOS of the corner states (a) at $\theta = \pi/4$ and (b) at $\theta = 5\pi/4$. These two are related by a single-exchange operation. Cyan arrows show the direction of the B field. (c) Impedance is the same at $\theta = \pi/4$ and $5\pi/4$. (d) LDOS of the corner states for $\pi/4 < \theta < 9\pi/4$, and their braiding. (e) Evolution of the Berry phase towards a double-exchange operation. (f) Energy spectrum evolution during the braiding. The Majorana corner states in red remains to be separated from the bulk spectrum in blue.

the LDOS and the impedance at $\theta = \pi/4, 5\pi/4$ in Fig.4(a)–(c), where the zero-energy corner states are clearly observed. See the LDOS at other values of θ elsewhere.

The zero-energy corner states subject to the PHS are Majorana states in condensed matter physics. A key question is whether they may be called Majorana states in electric circuits. Majorana particles are known to be Ising anyons possessing the property $\sigma^2 = -1$, where σ denotes the single-exchange operation^{1,4}. It is well known that only fermions and bosons are possible in 3D, for which $\sigma^2 = 1$. On the other hand, anyons are possible only in 2D. We recognize that this anyonic property is most important as a characteristics of Majorana states for future application to quantum computers.

We investigate the braiding for a pair of corner states. By increasing θ continuously from $\pi/4$ to $5\pi/4$ ($9\pi/4$), we can exchange the position of two corner states once (twice) as in Fig.4(d). The corner states remain to be zero-energy states with a finite gap during the process, as shown in Fig.4(f). Thus, they remain well separated from the bulk bands during the exchange of the two corner states. The key property is how the wave function changes as θ increases. Note that the phase of the wave function is observable by the phase shift in the electric circuit.

Let $|\psi_\alpha(\theta)\rangle$ be an eigenstate of $H_{\tau Z}^{\text{BHZ}}(\theta)$. When we increase θ adiabatically, the wave function $|\psi_\alpha(\theta)\rangle$ develops as^{1,4,40}

$$|\psi_\alpha(\theta)\rangle = \sum_{\beta=1,2} e^{i\Gamma_{\alpha\beta}(\theta)} |\psi_\beta(\pi/4)\rangle, \quad (11)$$

where $\Theta = \theta - \pi/4$, and $\Gamma_{\alpha\beta}(\Theta)$ is the Berry phase,

$$\Gamma_{\alpha\beta}(\Theta) = i \int_{\pi/4}^{\pi/4+\Theta} \langle \psi_\alpha(\theta) | \partial_\theta | \psi_\beta(\theta) \rangle d\theta. \quad (12)$$

There are two-fold degenerate zero-energy corner states at $\theta = \pi/4$. Since these two states are well separated as in Fig.4(a), we may label them by $\alpha = 1, 2$. Furthermore, we may construct the eigenfunctions continuous in θ such that $\langle \psi_\alpha(\theta) | \psi_\beta(\theta) \rangle = \delta_{\alpha\beta}$ for any value of θ . Then, it follows that $\Gamma_{\alpha\beta}(\Theta)$ is diagonal; $\Gamma(\Theta) \equiv \Gamma_{11}(\Theta) = \Gamma_{22}(\Theta)$. We show a numerical result for $\Gamma(\Theta)$ in Fig.4(e). In particular, we obtain $\Gamma(2\pi) = \pi$.

The single and double exchanges correspond to the rotations $\Theta = \pi$ and $\Theta = 2\pi$, respectively. After the double exchange we obtain $\Gamma_{\alpha\beta}(2\pi) = \pi\delta_{\alpha\beta}$, which yields $|\psi_1\rangle \rightarrow -|\psi_1\rangle$ and $|\psi_2\rangle \rightarrow -|\psi_2\rangle$, or $\sigma^2 = -1$. Consequently, the braiding is satisfied by the corner states in electric circuits. Hence, let us call the zero-energy corner states Majorana states also in the electric-circuit formalism. We can check that the braiding is robust against disorders.

Non-Hermitian Majorana states: We have so far analyzed Hermitian models. It is easy to make a model non-Hermitian by introducing resistors and diodes into an electric circuit^{35,36}. Since we are interested in Majorana states, we only consider the systems respecting the PHS. The PHS is generalized straightforwardly to the non-Hermitian case. The Majorana particle is identical to its antiparticle. A new feature is that its energy is zero or pure imaginary.

A non-Hermitian model is either reciprocal or nonreciprocal. To make the analysis concrete, we explicitly consider a non-Hermitian Kitaev model respecting the PHS. The Hamiltonian (1) together with (2) and (3) is generalized as

$$H(k) = i\gamma\mathbb{I} + \begin{pmatrix} f(t^b, t^f; k) & g(\Delta^b, \Delta^f; k) \\ g(\Delta^{b*}, \Delta^{f*}; k) & -f(t^{b*}, t^{f*}; k) \end{pmatrix}, \quad (13)$$

with $f(t^b, t^f; k) = t^b e^{ik} + t^f e^{-ik} - \mu$, $g(\Delta^b, \Delta^f; k) = -i(\Delta^b e^{ik} - \Delta^f e^{-ik})$, and γ representing dissipation, where t^b (t^f) is a backward (forward) hopping amplitude, Δ^b (Δ^f) is a backward (forward) superconducting pairing amplitude, and μ is the chemical potential. Parameters t^b, t^f, Δ^b and Δ^f take complex values, while μ and γ take real values. It satisfies the PHS, $\Xi^{-1}H(k)\Xi = -H(-k)$, with $\Xi = \sigma_x K$.

By diagonalizing (13), the bulk gap is found to close at

$$|\mu| = |\text{Re}(t^b + t^f) \pm |\Delta^b - \Delta^f||. \quad (14)$$

Gap-closing points are not phase-transition points when skin edge states are present in non-Hermitian theory^{35,41-47}.

We seek for topological phases. The system remains to be in the class Z_2 even for the non-Hermitian system⁴⁸, and hence, the topological number is given by the Z_2 invariant ν in the original Kitaev model as

$$(-1)^\nu = -\text{sgn}[H_z(0)H_z(\pi)], \quad (15)$$

where H_z is the coefficient of σ_z by expanding H as $H(k) = \sum_{\alpha=0,x,y,z} H_\alpha(k)\sigma_\alpha$, and $k = 0, \pi$ are the PHS invariant momenta. The formula (15) is valid also for the non-Hermitian system because of the PHS. Calculating it explicitly

we find that

$$(-1)^\nu = \text{sgn} \left[[\text{Re}(t^b + t^f)]^2 - \mu^2 \right]. \quad (16)$$

It follows from (16) that there are two phases with the phase-transition points $\mu_\pm = \pm |\text{Re}(t^b + t^f)|$. The system is topological ($\nu = 1$) for $|\mu| < |\text{Re}(t^b + t^f)|$ and trivial ($\nu = 0$) for $|\mu| > |\text{Re}(t^b + t^f)|$. The justification of (16) as the topological number is made by confirming numerically the non-Hermitian bulk-edge correspondence^{35,42-46}. The gap-closing points (14) become identical to the topological phase-transition points μ_\pm when the system is reciprocal, $\Delta^b = \Delta^f$.

The LDOS is shown for all eigen-energies in Fig.2(a1)-(c1) by taking typical values of sample parameters in the Hermitian, reciprocal non-Hermitian and nonreciprocal non-Hermitian cases. The characteristic feature of the nonreciprocal non-Hermitian model is the emergence of skin edge states as in [Fig.2(c1)], where all the eigen states are localized at one edge, as was first found in the non-Hermitian Su-Schrieffer-Heeger model⁴²⁻⁴⁴. Namely, two topological edge states are mixed between themselves and furthermore they are mixed with the bulk states in the vicinity of one edge. This is also the case for the topological corner states in the nonreciprocal non-Hermitian BHZ model. The braiding becomes meaningless in the nonreciprocal non-Hermitian models because there are no separated corner states.

We may construct a reciprocal non-Hermitian model respecting the PHS, by inserting a resistor R to a capacitance C and an inductor L in series in Fig.3. The circuit Laplacian is obtained just by replacing $C \rightarrow (1/C + i\omega R)^{-1}$ and $\omega^2 L \rightarrow \omega^2 L - i\omega R$. We can check that the resultant non-Hermitian model is different from the original Hermitian model only by a pure imaginary shift. In such a case the braiding holds just as it is since the wave functions are not modified.

Discussion: We have shown that Majorana edge and corner states are simulated by electric circuits. The Majorana corner states emerge in electric circuits whose size is as small as $N = 4$, which is a benefit on future high-density applications. Majorana states will be a key for future topological quantum computations, where the essential property is the braiding between two Majorana states. Furthermore, various extensions are possible to electric circuits for such as the dimerized Kitaev model⁴⁹ and the Kitaev ladder model⁵⁰. Our results might open a new way for topological quantum computations based on Majorana states in electric circuits.

The author is very grateful to A. Kurobe for fruitful conversations on the subject, which motivated the present work. He is also thankful to Y. Tanaka and N. Nagaosa for helpful discussions on the subject. He also thanks to T. Pahomi and A. A. Soluyanov on discussions on the braiding of Majorana states. This work is supported by the Grants-in-Aid for Scientific Research from MEXT KAKENHI (Grants No. JP17K05490, No. JP15H05854 and No. JP18H03676). This work is also supported by CREST, JST (JPMJCR16F1 and JPMJCR1874).

- ¹ C. Nayak, S. H. Simon, A. Stern, M. Freedman, and S. Das Sarma, *Rev. Mod. Phys.* **80**, 1083 (2008).
- ² X.-L. Qi, S.-C. Zhang, *Rev. Mod. Phys.* **83**, 1057 (2011).
- ³ M. Sato and Y. Ando, *Rep. Prog. Phys.* **80**, 076501 (2017).
- ⁴ A. Kitaev, *Annals of Physics* **321**, 2 (2006).
- ⁵ Y. Kasahara, T. Ohnishi, Y. Mizukami, O. Tanaka, Sixiao Ma, K. Sugii, N. Kurita, H. Tanaka, J. Nasu, Y. Motome, T. Shibauchi, Y. Matsuda, *Nature* **559**, 227 (2018).
- ⁶ J. Alicea, *Rep. Prog. Phys.* **75**, 076501 (2012).
- ⁷ C. W.J. Beenakker, *Annu. Rev. Condens. Matter Phys.* **4**, 113 (2013).
- ⁸ S.R. Elliott and M. Franz, *Rev. Mod. Phys.* **87**, 137 (2015).
- ⁹ Z. Yan, F. Song, Z. Wang, *Phys. Rev. Lett.* **121**, 096803 (2018)
- ¹⁰ Q. Wang, C.-C. Liu, Y.-M. Lu, F. Zhang, *Phys. Rev. Lett.* **121**, 186801 (2018)
- ¹¹ Y. Volpez, D. Loss, J. Klinovaja, *Phys. Rev. Lett.* **122**, 126402 (2019)
- ¹² Y. Wang, M. Lin, T. L. Hughes, *Phys. Rev. B* **98**, 165144 (2018)
- ¹³ T. Liu, J. J. He, F. Nori, *Phys. Rev. B* **98**, 245413 (2018)
- ¹⁴ X. Zhu, *Phys. Rev. B* **97**, 205134 (2018)
- ¹⁵ T. E. Pahomi, M. Sigrist, A. A. Soluyanov, arXiv:1904.07822
- ¹⁶ S. Malzard, C. Poli, H. Schomerus, *Phys. Rev. Lett.* **115**, 200402 (2015).
- ¹⁷ P. San-Jose, J. Cayao, E. Prada and R. Aguado, *Scientific Reports* **6**, 21427 (2016)
- ¹⁸ C. Yuce, *Phys. Rev. A* **93**, 062130 (2016).
- ¹⁹ C. Li, Liang. Jin, Z. Song, cond-mat/arXiv:1710.07794.
- ²⁰ C. Li, X. Z. Zhang, G. Zhang, Z. Song, *Phys. Rev. B* **97**, 115436 (2018).
- ²¹ E. Cobanera, A. Alase, G. Ortiz, L. Viola, *Phys. Rev. B* **98**, 245423 (2018).
- ²² A. A. Zyuzin, P. Simon, *Phys. Rev. B* **99**, 165145 (2019)
- ²³ J. Avila, F. Penaranda, E. Prada, P. San-Jose, R. Aguado, cond-mat/arXiv:1807.04677
- ²⁴ K. Kawabata, Y. Ashida, H. Katsura, M. Ueda, *Phys. Rev. B* **98**, 085116 (2018).
- ²⁵ K. Kawabata, S. Higashikawa, Z. Gong, Y. Ashida, M. Ueda, *Nat. Commun.* **10**, 297 (2019).
- ²⁶ C. H. Lee, S. Imhof, C. Berger, F. Bayer, J. Brehm, L. W. Molenkamp, T. Kiessling and R. Thomale, *Communications Physics*, **1**, 39 (2018).
- ²⁷ T. Helbig, T. Hofmann, C. H. Lee, R. Thomale, S. Imhof, L. W. Molenkamp and T. Kiessling, *Phys. Rev. B* **99**, 161114 (2019).
- ²⁸ Y. Lu, N. Jia, L. Su, C. Owens, G. Juzeliunas, D. I. Schuster and J. Simon, *Phys. Rev. B* **99**, 020302 (2019).
- ²⁹ K. Luo, R. Yu and H. Weng, *Research* (2018), ID 6793752.
- ³⁰ K. Luo, J. Feng, Y. X. Zhao, and R. Yu, arXiv:1810.09231.
- ³¹ S. Imhof, C. Berger, F. Bayer, J. Brehm, L. Molenkamp, T. Kiessling, F. Schindler, C. H. Lee, M. Greiter, T. Neupert, R. Thomale, *Nat. Phys.* **14**, 925 (2018).
- ³² M. Serra-Garcia, R. Susstrunk and S. D. Huber, *Phys. Rev. B* **99**, 020304 (2019)
- ³³ M. Ezawa, *Phys. Rev. B* **98**, 201402(R) (2018).
- ³⁴ T. Hofmann, T. Helbig, C. H. Lee, M. Greiter, R. Thomale, arXiv:1809.08687.
- ³⁵ M. Ezawa, cond-mat/arXiv:1810.04527. to be published in *PRB*(R) (2019)
- ³⁶ M. Ezawa, *Phys. Rev. B* **99**, 121411(R) (2019)
- ³⁷ J. Alicea, Y. Oreg, G. Refael, F. von Oppen and M.P.A. Fisher, *Nat. Phys.* **7**, 412 (2011)
- ³⁸ B. A. Bernevig, T. L. Hughes, and S.-C. Zhang, *Science* **314**, 1757 (2006).
- ³⁹ M. Ezawa, *Phys. Rev. Lett.* **121**, 116801 (2018)
- ⁴⁰ S. D. Sarma, M. Freedman, and C. Nayak, *npj Quantum Inf.* **1**, 15001 (2015)
- ⁴¹ Y. Xiong, *J. Physics Communications* **2**, 035043 (2018).
- ⁴² S. Yao and Z. Wang, *Phys. Rev. Lett.* **121**, 086803 (2018).
- ⁴³ S. Yao, F. Song and Z. Wang, *Phys. Rev. Lett.* **121**, 136802 (2018)
- ⁴⁴ F. K. Kunst, E. Edvardsson, J. C. Budich and E. J. Bergholtz, *Phys. Rev. Lett.* **121**, 026808 (2018).
- ⁴⁵ C. H. Lee, R. Thomale, *Phys. Rev. B* **99**, 201103(R) (2019).
- ⁴⁶ L. Jin and Z. Song, *Phys. Rev. B* **99**, 081103 (2019).
- ⁴⁷ C. H. Lee, L. Li and J. Gong, cond-mat/arXiv:1810.11824.
- ⁴⁸ K. Kawabata, K. Shiozaki, M. Ueda, M. Sato, cond-mat/arXiv:1812.09133
- ⁴⁹ R. Wakatsuki, M. Ezawa, Y. Tanaka and N. Nagaosa, *Phys. Rev. B* **90**, 014505 (2014).
- ⁵⁰ R. Wakatsuki, M. Ezawa, N. Nagaosa, *Phys. Rev. B* **89**, 174514 (2014).